Geochemical Perspectives Letters

Deformation modulates helium diffusion behaviour in apatite

M.M. Tremblay[1*], A.K. Fayon[2], H. Guo[1], P.K. Zeitler[3], B.D. Idleman[3]

OPEN ACCESS

https://doi.org/10.7185/geochemlet.2523

Abstract

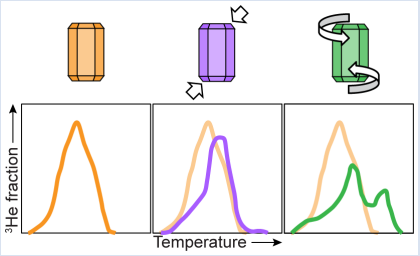

Utilising the apatite (U-Th)/He thermochronometer to infer the thermal histories of geologic materials requires understanding the factors that influence helium diffusion kinetics. Here, we demonstrate that deformation in apatite modulates helium diffusion behaviour. We deformed single crystal Durango apatite under compression and torsion, used electron microscopy to characterise the deformation, and measured the evolution of ^{3}He and ^{4}He released during stepwise heating experiments on proton-irradiated fragments of the deformed crystals. Fragments deformed under compression contained distributed dislocations and resulted in mostly unimodal helium release comparable to undeformed, unannealed Durango apatite, while fragments deformed to higher stress under torsion contain a higher dislocation density, developed subgrain boundaries defined by dislocation arrays, and exhibited multimodal helium release, comparable to results from continuous ramped heating analysis of some natural apatite samples. We conclude that deformation-induced dislocations can modulate helium diffusion behaviour by impeding helium diffusion and functioning as diffusion sinks, and are likely an important source of (U-Th)/He date overdispersion in natural samples.

Received 4 February 2025 | Accepted 13 June 2025 | Published 8 July 2025

Introduction

The apatite (U-Th)/He thermochronometer is widely utilised for inferring the low temperature thermal histories of rocks in relation to landscape evolution and tectonic processes (*e.g.*, Gautheron and Zeitler, 2020). However, apatite (U-Th)/He dates from individual samples are often overdispersed, limiting the thermal history information that can be inferred. This date overdispersion cannot be fully explained by the well documented effects of grain size (*e.g.*, Reiners and Farley, 2001), parent nuclide zonation (*e.g.*, Meesters and Dunai, 2002; Hourigan *et al.*, 2005; Sousa *et al.*, 2024), or radiation damage on helium diffusion kinetics (*e.g.*, Shuster *et al.*, 2006; Flowers *et al.*, 2009; Gautheron *et al.*, 2013; Willett *et al.*, 2017).

The development of continuous ramped heating (CRH) measurements (Idleman *et al.*, 2018), wherein radiogenic ^{4}He is continuously measured during progressive heating to higher temperatures, has provided new insights into grain-specific helium diffusion behaviour in apatite. Some apatite grains exhibit unimodal helium release over the temperature range expected from the helium diffusion kinetics for the reference material Durango apatite, the basis for existing models of helium diffusion in apatite (*e.g.*, Flowers *et al.*, 2009). However, other grains exhibit helium release peaks at multiple temperatures and/or significantly different temperatures than would be predicted from Durango apatite kinetics (*e.g.*, Guo *et al.*, 2021; Idleman *et al.*, 2018; McDannell *et al.*, 2018). Most notably, apatite grains from the KTB borehole, sampled at depths where no radiogenic helium is predicted to be retained due to high temperatures, can contain substantial ^{4}He and exhibit complex ^{4}He release patterns (Guo *et al.*, 2024). While complex helium behaviour observed in CRH measurements has broadly been attributed to imperfections in the crystal lattice of apatite that act as helium 'sinks' (*e.g.*, Guo *et al.*, 2021, 2024), the origin and nature of such imperfections remains an open question. Vacancies have been proposed to impact helium retentivity in apatite (Gerin *et al.*, 2017) but not necessarily to cause complex helium diffusion behaviour. Here, we present laboratory experiments that investigate whether deformation-induced imperfections can function as helium sinks in apatite and explain the range of kinetics observed across many grains that is unexplained by radiation damage (Guo *et al.*, 2021). By experimentally deforming Durango apatite – a sample for which helium behaviour is well characterised and simple in the absence of deformation – we can directly link deformation features we generate to their effects on helium behaviour.

Methods

We deformed cylinders of single crystal Durango apatite in a Paterson gas-medium apparatus under two different experimental conditions. Experiment PI2014 was conducted in compression with the crystal cut such that the basal plane was oriented 45° to the maximum compressive stress. Experiment PT1547 was conducted in torsion with the crystal oriented such that the *c*-axis was parallel to the twist axis resulting in shear along the basal plane, analogous to how apatite would deform under shear in geologic settings. The deformation experiments

1. Department of Earth, Atmospheric, and Planetary Sciences, Purdue University, West Lafayette, IN 47907, USA
2. Department of Earth and Environmental Sciences, University of Minnesota - Twin Cities, Minneapolis, MN 55455, USA
3. Department of Earth and Environmental Sciences, Lehigh University, Bethlehem, PA 18015, USA
* Corresponding author (email: tremblam@purdue.edu)

were conducted at 300 MPa confining pressure and 1100 °C for 2 hours (PI2014) and 5 hours (PT1547). Deformed samples were characterised using backscatter electron imaging, electron backscatter diffraction (EBSD) analysis, and chemical etching. Full deformation experiment and sample characterisation details are provided in the Supplementary Information.

We anticipated that radiogenic ^{4}He in the deformed apatite crystals would be diffusively lost during the high temperature deformation experiments. Therefore, we needed to introduce helium into the deformed crystals to understand the effects of the deformation on helium behaviour. To achieve this, we crushed the deformed crystals into ~100–500 μm fragments and irradiated both deformed and undeformed, unannealed Durango apatite fragments with protons. Proton irradiation produces a uniform, high concentration of ^{3}He, enabling diffusion experiments with many heating steps to be carried out on individual mineral grains or fragments (*e.g.*, Shuster *et al.*, 2004). Following proton irradiation, stepwise heating diffusion experiments on individual fragments were carried out in the noble gas thermochronology facility at Purdue University. Full details about the proton irradiation and diffusion experiments are provided in the Supplementary Information.

Results

Experimentally induced deformation. Both experimentally deformed samples exhibit crystal defects but differ in both the density and organisation of defects present. PI2014, deformed in compression, exhibits dislocations within the basal plane with minor lattice distortion (Fig. 1a,b): a dislocation density of ~10^{10} m^{-2} is necessary to account for the observed lattice curvature in EBSD data (Pantleon, 2008). This produces a very subtle 'tiger-stripe' microtexture in the EBSD map (Fig. 1a), comparable to textures seen in naturally deformed apatite samples (*e.g.*, Odlum and Stockli, 2020). The etched surface of this sample shows a relatively uniform distribution of dislocations at an angle to the surface of the grain (Fig. 1c).

PT1547, deformed in torsion, exhibits both dislocations and bands of subgrains whose boundaries are defined by dislocation arrays subparallel to and within the basal plane (Fig. 2). Lattice curvature measured from EBSD data for PT1547 requires a dislocation density of ~10^{11} and up to 10^{12} m^{-2} across subgrain boundaries, at least an order of magnitude greater than the dislocation density for PI2014. In addition to the lattice curvature, subgrains are observed in PT1547 with misorientations between 2 and 8° (Fig. 2b,c). These subgrains are not pervasive but are visible in both EBSD data and etched surfaces when oriented such that the *c*-axis is near-orthogonal to the polished surface (Fig. 2b; see also Supplementary Information) and are characterised by a higher dislocation density relative to other parts of the sample. The presence of subgrains and 5–15° of disorientation, comparable to the deformation we produced in PT1547,

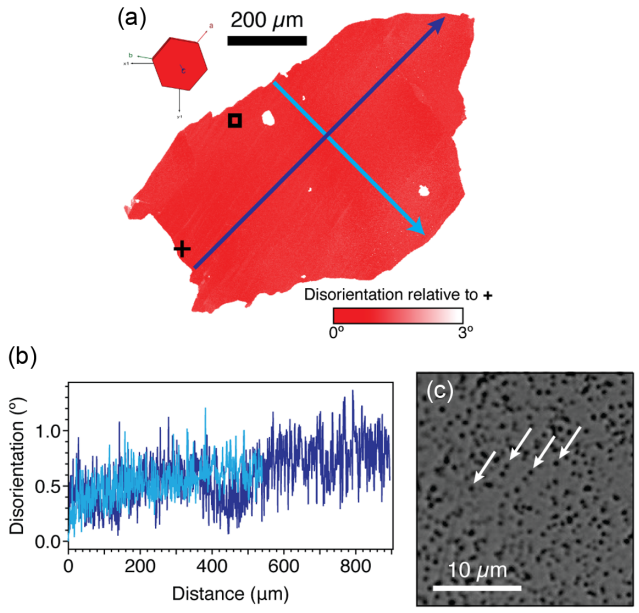

Figure 1 Damage induced in Durango apatite deformed under compression in experiment PI2014. **(a)** EBSD disorientation map and **(b)** line scans across a deformed fragment. **(c)** Reflected light image after 10–20 seconds of etching in 0.5 M HNO_3 to reveal defects. Area corresponds to the black box in **(a)**. Arrows highlight several dislocation etch pits visible in this surface. Note that the specific fragment used for the diffusion experiment was plucked during polishing, so this is a different fragment. Note also the crystallographic orientation at which each fragment was mounted, which affects the degree of disorientation observed (see also Fig. S-1). Additional EBSD data from PI2014 deformed material are shown in Figure S-3.

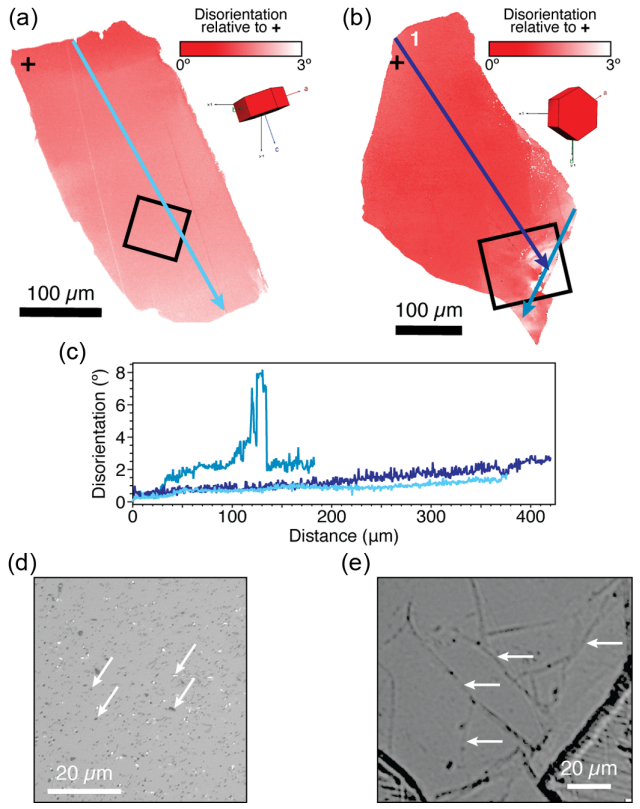

Figure 2 Damage induced in Durango apatite deformed under torsion in experiment PT1547. **(a, b)** EBSD disorientation maps and **(c)** line scans across the two fragments degassed in diffusion experiments. **(d, e)** Reflected light images after etching in 0.5 M HNO_3 for 10–20 seconds to reveal defects, with arrows highlighting **(d)** etched dislocations and **(e)** etched subgrain boundaries. Bright dislocations in **(d)** are subparallel to the etched surface. The fragment used for the diffusion experiment in Figures 3 and 4 is shown in **(a, d)**, while the fragment used for the replicate experiment in Figure S-5 is shown in **(b, e)**. Note the crystallographic orientation at which each fragment was mounted, which affects the degree of disorientation observed and the likelihood of observing subgrain boundaries (see also Fig. S-1). Additional EBSD data from PT1547 deformed material are shown in Figure S-4.

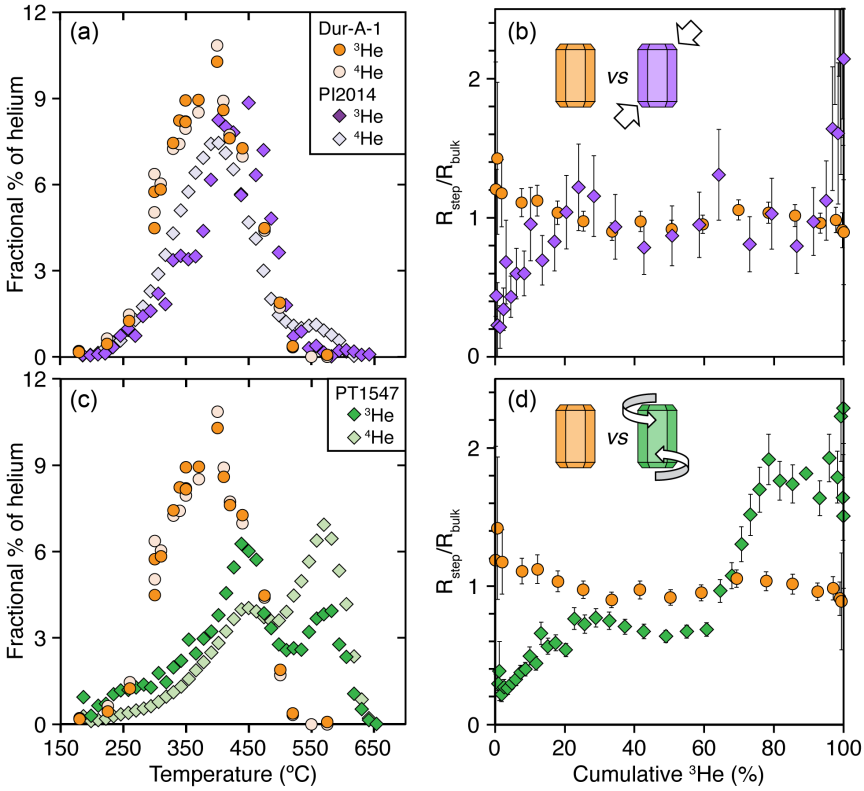

Figure 3 Step heating experiments on Durango apatite fragments deformed under **(a, b)** compression (PI2014) or **(c, d)** torsion (PT1547), compared to undeformed, unannealed Durango apatite (DUR-A-1). **(a, c)** Fractional release of ^{3}He and ^{4}He as a function of temperature. **(b, d)** Step ^{4}He/^{3}He normalised to the cumulative ^{4}He/^{3}He (R_{step}/R_{bulk}), plotted with 1σ uncertainties, as a function of cumulative ^{3}He release.

have been observed in naturally deformed apatite samples (*e.g.*, Ribeiro *et al.*, 2020; Odlum *et al.*, 2022).

Stepwise degassing experiments. Figure 3 shows results from stepwise degassing experiments on individual fragments in two formats: as a fraction of helium released as a function of temperature (Fig. 3a,c), which are analogous to CRH analysis incremental helium loss curves, and as ^{4}He/^{3}He ratios as a function of cumulative ^{3}He release (Fig. 3b,d), comparable to conventional ^{4}He/^{3}He datasets. A second experiment on PT1547 is shown in the Supplementary Information. For undeformed, unannealed Durango apatite (DUR-A-1), we observed a unimodal release of both ^{3}He and ^{4}He with nearly identical release peaks at ~400 °C (Fig. 3a,c), corresponding to an invariant ^{4}He/^{3}He (Fig. 3b,d). These observations are expected for Durango apatite based on previous experiments characterising its diffusion kinetics (see Supplementary Information; *e.g.*, Farley, 2000; Shuster *et al.*, 2004) as well as CRH measurements (Idleman *et al.*, 2018; McDannell *et al.*, 2018). Our experiments on deformed Durango fragments exhibit different behaviour. For Durango apatite deformed under compression (PI2014), we observe a mostly unimodal release of both ^{3}He and ^{4}He, similar to DUR-A-1 (Fig. 3a), with a minor second peak observed at >500 °C. The ^{4}He/^{3}He increases in this experiment over the first ~30 % of the ^{3}He release and then remains constant (Fig. 3b). The helium diffusion kinetics derived from the proton-induced ^{3}He in PI2014 are similar to the kinetics of Durango apatite reported by Farley (2000) and measured in our DUR-A-1 experiment (Figs. 4a,b, S-7), but substantially different from the helium diffusion kinetics measured in Durango apatite with annealed radiation damage (Figs. S-6, S-7).

For Durango apatite deformed under torsion (PT1547), we observe two prominent, coincident release peaks for ^{3}He and ^{4}He, with the second peak occurring at higher temperatures (>500 °C) than in DUR-A-1 (Figs. 3c, S-5). The ^{3}He release fraction corresponding to the first peak is larger than the second, higher temperature peak, while the opposite was observed for ^{4}He. The resulting ^{4}He/^{3}He evolution in this experiment has two discrete benches or plateaus (Fig. 3d), and the diffusion kinetics derived from the proton-induced ^{3}He are markedly different from the kinetics of undeformed, unannealed Durango apatite (Fig. 4a,c). Specifically, we observe higher apparent diffusivities for the first ~20 % of the ^{3}He released and a pair of lower apparent diffusivity trends for the remaining ^{3}He released.

Discussion

Deformation-induced helium diffusion sinks and changes in volume diffusion kinetics. The deformation features we produced in PI2014 and PT1547 are comparable to features in naturally deformed apatite observed in petrochronologic studies (*e.g.*, Odlum and Stockli, 2020; Ribeiro *et al.*, 2020; Odlum *et al.*, 2022). It is important to note that the dislocations produced in the deformation experiments can migrate during hydrostatic conditions (*e.g.*, glide or climb; Passchier and Trouw, 2005) but do not anneal like radiation damage, and during the heating conditions of our diffusion experiments were thermally persistent. This is evidenced by the dislocations and subgrain boundaries retained in the PT1547 diffusion experiment fragments (Fig. 2), as well as observations from the apatite fission track community that dislocations persist even after fission tracks have been annealed (*e.g.*, Bertel and Märk, 1983). While it has been hypothesised that deformation modifies helium behaviour in apatite (*e.g.*, Fayon and Hansen, 2015; McDannell *et al.*, 2018; Fayon and Cherniak, 2021; Guo *et al.*, 2024), the impact of deformation has not been clearly documented in previous studies.

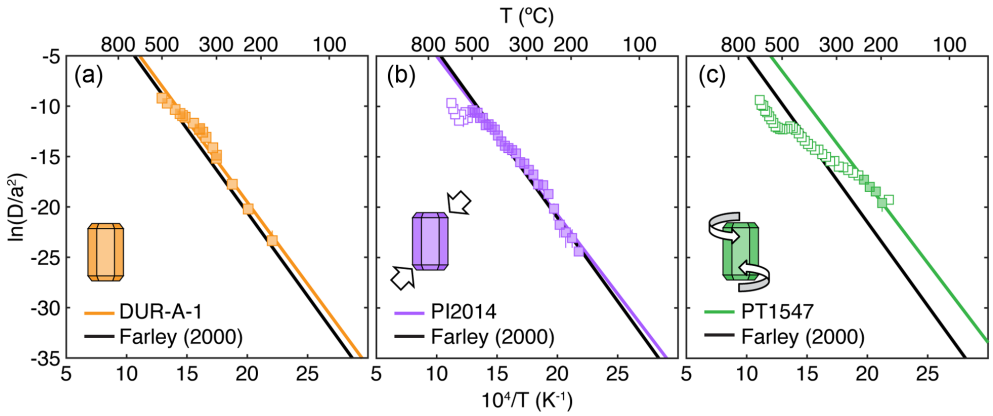

Figure 4 Arrhenius plot for diffusion of proton-induced ^{3}He in **(a)** DUR-A-1, **(b)** PI2014, and **(c)** PT1547, compared to the helium diffusion kinetics for Durango apatite reported by Farley (2000), scaled to the spherical equivalent radii of each fragment. Lines are fit to the filled data points. Where not visible, uncertainties in ln(D/a^2) values are smaller than the symbols plotted.

PI2014 contains a uniform distribution of dislocations (Fig. 1) and exhibits a mostly unimodal helium release behaviour that is comparable to undeformed, unannealed Durango apatite (Figs. 3a,b, 4b), albeit with some apparent diffusive rounding of radiogenic ^{4}He (Fig. 3b). The presence of a minor second release peak at temperatures >500 °C suggests that the dislocations in PI2014 have induced some complex helium release behaviour, albeit limited compared to PT1547. Additionally, the similarity of helium diffusion kinetics in PI2014 and in undeformed, unannealed Durango apatite (Figs. 4a,b, S-7) suggests that the dislocations produced in PI2014 impeded helium diffusion in a manner comparable to radiation damage (*e.g.*, Shuster *et al.*, 2006; Flowers *et al.*, 2009). If this were not the case, we would expect the ^{3}He diffusion kinetics in PI2014 to be less retentive and more similar to the diffusion kinetics of Durango apatite in which radiation damage had been experimentally annealed (Figs. S-6, S-7; Shuster and Farley, 2009), since radiation damage present in the PI2014 starting material was annealed at the high temperatures of the deformation experiment.

The higher density of dislocations and dislocation arrays comprising subgrain boundaries in PT1547 (Figs. 2, S-4) are associated with anomalous, significant multimodal helium release behaviour (Fig. 3c,d), reminiscent of multiple diffusion domain behaviour commonly observed for ^{40}Ar/^{39}Ar spectra from K Feldspars (*e.g.*, Harrison and Lovera, 2014) and comparable to the CRH evolution of ^{4}He in some natural apatite samples (*e.g.*, Guo *et al.*, 2024). It is important to note that the proton-induced ^{3}He has a uniform spatial distribution at the beginning of a stepwise degassing experiment. Therefore, the multimodal release of ^{3}He we observe can only result from the redistribution of ^{3}He during the degassing experiment. The high apparent diffusivities characterising the initial ^{3}He release in PT1547 (Fig. 4b) may result from fractures we did not detect when selecting this fragment that essentially reduce the effective diffusion length scale for a small portion of the fragment analysed. Alternatively, these high diffusivities could reflect a change in the volume diffusion kinetics induced by deformation in at least part of the sample.

The high apparent initial diffusivities in PT1547 transition to diffusivities consistent with the helium diffusion kinetics for undeformed Durango apatite (Fig. 4b), corresponding to the first 'plateau' we see in the ^{4}He/^{3}He evolution (Fig. 3d). A significant proportion of the ^{3}He is then retained until higher temperatures than we would expect from undeformed Durango apatite kinetics (Figs. 3c, 4b), corresponding to the second 'plateau' we see in the ^{4}He/^{3}He evolution (Fig. 3d). Guo *et al.* (2024) hypothesised that this could occur if ^{3}He encountered lattice imperfections that acted as helium sinks, such that there was an additional kinetic barrier for helium to continue diffusing interstitially once it encountered a sink in the degassing experiment, resulting in a higher temperature release of ^{3}He. The corresponding second release peak for ^{4}He, which corresponds to larger gas release fractions than ^{3}He, further suggests that trapping of radiogenic ^{4}He occurred during the deformation experiment, in addition to trapping during the subsequent diffusion experiment. Overall, our observations from PT1547 suggest that a locally high dislocation density (*i.e.* relative to PI2014) or array of dislocations can create diffusion sinks related to crystal-plastic deformation, which is perhaps not surprising, as extended defects have previously been suggested to impede helium diffusion and/or trap helium in apatite and other minerals based on first principles calculations (*e.g.*, Domingos *et al.*, 2020; Gautheron *et al.*, 2020; Gerin *et al.*, 2017).

Farley (2000) predicted that helium diffusion kinetics in apatite should vary based on the presence of crystal imperfections including, but not limited to, radiation damage, and Guo *et al.* (2021) demonstrated that this kinetics variation does occur and cannot be completely explained by different combinations of grain size and radiation damage. Our paired deformation–^{4}He/^{3}He experiments support the hypothesis that deformation-induced extended defects in apatite impact the behaviour of radiogenic ^{4}He in natural apatite samples. Defects can function as reversible, temperature dependent diffusion 'sinks' that impede the diffusive loss of ^{4}He over a sample's geologic thermal history and may also alter volume diffusion kinetics. Because these defects form during crystal-plastic deformation (*e.g.*, Nakano *et al.*, 2001; Saka *et al.*, 2008; Odlum *et al.*, 2022), we can infer that, in natural samples, such defects will form during the high temperature portion of an apatite sample's geologic history, before significant radiogenic ^{4}He accumulation occurs. The impact of such defects on helium behaviour likely contributes to apatite (U-Th)/He date overdispersion, specifically resulting in dispersion toward older ages (*e.g.*, Guo *et al.*, 2021) compared to what is expected given current diffusion models. Importantly, detecting such behaviour requires obtaining information about the behaviour of helium release during laboratory degassing, either through ^{4}He/^{3}He experiments like those presented here or through CRH measurements (Idleman *et al.*, 2018). Further work is necessary to evaluate if a constitutive relationship between deformation and helium retentivity can be developed and broadly applied to (U-Th)/He datasets.

Conclusions

We demonstrate with experiments that dislocations produced during plastic deformation of apatite can operate as diffusion sinks for helium. Retention of helium to higher temperatures in such sinks is likely an important source of (U-Th)/He date overdispersion in natural apatite samples, and incorporating the effects of deformation-induced helium sinks into our apatite helium diffusion models will be important for making accurate thermal history interpretations from many (U-Th)/He datasets.

Acknowledgements

This research was supported by a Sloan Research Fellowship awarded to MMT by the Alfred P. Sloan Foundation (FG-2022-18729). Apatite deformation experiments were carried out with U.S. National Science Foundation grants to AKF (EAR-1727203) and PKZ and BDI (EAR-1726350). We thank L. Hansen, A. Dillman, and H. Wiesman for helpful discussions, W. Nachlas for assistance with EBSD data collection, three anonymous reviewers for their constructive feedback, and F. McCubbin for editorial handling.

Editor: Francis McCubbin

Additional Information

Supplementary Information accompanies this letter at https://www.geochemicalperspectivesletters.org/article2523.

Cite this letter as: Tremblay, M.M., Fayon, A.K., Guo, H., Zeitler, P.K., Idleman, B.D. (2025) Deformation modulates helium diffusion behaviour in apatite. *Geochem. Persp. Let.* 35, 49–54. https://doi.org/10.7185/geochemlet.2523

References

Bertel, E., Märk, T.D. (1983) Fission tracks in minerals: Annealing kinetics, track structure and age correction. *Physics and Chemistry of Minerals* 9, 197–204. https://doi.org/10.1007/BF00311955

Domingos, R., Tremblay, M.M., Shuster, D.L., Militzer, B. (2020) Simulations and Experiments Reveal Effect of Nanopores on Helium Diffusion in Quartz. *ACS Earth and Space Chemistry* 4, 1906–1912. https://doi.org/10.1021/acsearthspacechem.0c00187

Farley, K.A. (2000) Helium diffusion from apatite: General behavior as illustrated by Durango fluorapatite. *Journal of Geophysical Research: Solid Earth* 105, 2903–2914. https://doi.org/10.1029/1999JB900348

Fayon, A.K., Cherniak, D.J. (2021) Helium diffusion in experimentally deformed Durango apatite single crystals. *17th International Conference on Thermochronology* [Abstract], 12–17 September 2021, Santa Fe, NM.

Fayon, A.K., Hansen, L. (2015) Effects of deformation on apatite (U-Th)/He single-grain ages. *2015 GSA Annual Meeting* [Abstract], 1–4 November 2015, Baltimore, MD, 104–11.

Flowers, R.M., Ketcham, R.A., Shuster, D.L., Farley, K.A. (2009) Apatite (U–Th)/He thermochronometry using a radiation damage accumulation and annealing model. *Geochimica et Cosmochimica Acta* 73, 2347–2365. https://doi.org/10.1016/j.gca.2009.01.015

Gautheron, C., Zeitler, P.K. (2020) Noble Gases Deliver Cool Dates from Hot Rocks. *Elements* 16, 303–309. https://doi.org/10.2138/gselements.16.5.303

Gautheron, C., Barbarand, J., Ketcham, R.A., Tasson-Got, L., van der Beek, P., Pagel, M., Pinna-Jamme, R., Couffignal, F., Fialin, M. (2013) Chemical influence on α-recoil damage annealing in apatite: Implications for (U–Th)/He dating. *Chemical Geology* 351, 257–267. https://doi.org/10.1016/j.chemgeo.2013.05.027

Gautheron, C., Djimbi, D.M., Roques, J., Balout, H., Ketcham, R.A., Simoni, E., Pik, R., Seydoux-Guillaume, A.-M., Tassan-Got, L. (2020) A multi-method, multi-scale theoretical study of He and Ne diffusion in zircon. *Geochimica et Cosmochimica Acta* 268, 348–367. https://doi.org/10.1016/j.gca.2019.10.007

Gerin, C., Gautheron, C., Oliviero, E., Bachelet, C., Djimbi, D.M., Seydoux-Guillaume, A.-M., Tassan-Got, L., Sarda, P., Roques, J., Garrido, F. (2017) Influence of vacancy damage on He diffusion in apatite, investigated at atomic to mineralogical scales. *Geochimica et Cosmochimica Acta* 197, 87–103. https://doi.org/10.1016/j.gca.2016.10.018

Guo, H., Zeitler, P.K., Idleman, B.D., Fayon, A.K., Fitzgerald, P.G., McDannell, K.T. (2021) Helium diffusion systematics inferred from continuous ramped heating analysis of Transantarctic Mountains apatites showing age overdispersion. *Geochimica et Cosmochimica Acta* 310, 113–130. https://doi.org/10.1016/j.gca.2021.07.015

Guo, H., Zeitler, P.K., Idleman, B.D. (2024) Behavior of helium diffusion sinks in apatite: Evidence from continuous ramped heating analysis of borehole and well-characterized samples. *Earth and Planetary Science Letters* 641, 118828. https://doi.org/10.1016/j.epsl.2024.118828

Harrison, T.M., Lovera, O.M. (2014) The multi-diffusion domain model: past, present and future. In: Jourdan, F., Mark, D.F., Verati, C. (Eds.) *Advances in $^{40}Ar/^{39}Ar$ Dating: From Archaeology to Planetary Sciences*. Geological Society of London, London, Special Publication 378, 91–106. https://doi.org/10.1144/SP378.9

Hourigan, J.K., Reiners, P.W., Brandon, M.T. (2005) U-Th zonation-dependent alpha-ejection in (U-Th)/He chronometry. *Geochimica et Cosmochimica Acta* 69, 3349–3365. https://doi.org/10.1016/j.gca.2005.01.024

Idleman, B.D., Zeitler, P.K., McDannell, K.T. (2018) Characterization of helium release from apatite by continuous ramped heating. *Chemical Geology* 476, 223–232. https://doi.org/10.1016/j.chemgeo.2017.11.019

McDannell, K.T., Zeitler, P.K., Janes, D.G., Idleman, B.D., Fayon, A.K. (2018) Screening apatites for (U-Th)/He thermochronometry via continuous ramped heating: He age components and implications for age dispersion. *Geochimica et Cosmochimica Acta* 223, 90–106. https://doi.org/10.1016/j.gca.2017.11.031

Meesters, A.G.C.A., Dunai, T.J. (2002) Solving the production–diffusion equation for finite diffusion domains of various shapes: Part II. Application to cases with α-ejection and nonhomogeneous distribution of the source. *Chemical Geology* 186, 57–73. https://doi.org/10.1016/S0009-2541(01)00423-5

Nakano, T., Awazu, T., Umakoshi, Y. (2001) Plastic deformation and operative slip system in mineral fluorapatite single crystal. *Scripta Materialia* 44, 811–815. https://doi.org/10.1016/S1359-6462(00)00656-4

Odlum, M.L., Stockli, D.F. (2020) Geochronologic constraints on deformation and metasomatism along an exhumed mylonitic shear zone using apatite U-Pb, geochemistry, and microtextural analysis. *Earth and Planetary Science Letters* 538, 116177. https://doi.org/10.1016/j.epsl.2020.116177

Odlum, M.L., Levy, D.A., Stockli, D.F., Stockli, L.D., DesOrmeau, J.W. (2022) Deformation and metasomatism recorded by single-grain apatite petrochronology. *Geology* 50, 697–703. https://doi.org/10.1130/G49809.1

Pantleon, W. (2008) Resolving the geometrically necessary dislocation content by conventional electron backscattering diffraction. *Scripta Materialia* 58, 994–997. https://doi.org/10.1016/j.scriptamat.2008.01.050

Passchier, C.W., Trouw, R.A.J. (2005) *Microtectonics*. Second Edition, Springer, Berlin.

Reiners, P.W., Farley, K.A. (2001) Influence of crystal size on apatite (U–Th)/He thermochronology: an example from the Bighorn Mountains, Wyoming. *Earth and Planetary Science Letters* 188, 413–420. https://doi.org/10.1016/S0012-821X(01)00341-7

Ribeiro, B.V., Lagoeiro, L., Faleiros, F.M., Hunter, N.J.R., Queiroga, G., Raveggi, M., Cawood, P.A., Finch, M., Campanha, G.A.C. (2020) Strain localization and fluid-assisted deformation in apatite and its influence on trace elements and U–Pb systematics. *Earth and Planetary Science Letters* 545, 116421. https://doi.org/10.1016/j.epsl.2020.116421

Saka, H., Goto, D., Moon, W.-J. (2008) Dislocations in plastically deformed apatite. *Journal of Materials Science* 43, 3234–3239. https://doi.org/10.1007/s10853-008-2551-z

Shuster, D.L., Farley, K.A. (2009) The influence of artificial radiation damage and thermal annealing on helium diffusion kinetics in apatite. *Geochimica et Cosmochimica Acta* 73, 183–196. https://doi.org/10.1016/j.gca.2008.10.013

Shuster, D.L., Farley, K.A., Sisterson, J.M., Burnett, D.S. (2004) Quantifying the diffusion kinetics and spatial distributions of radiogenic ^{4}He in minerals

containing proton-induced ^{3}He. *Earth and Planetary Science Letters* 217, 19–32. https://doi.org/10.1016/S0012-821X(03)00594-6

Shuster, D.L., Flowers, R.M., Farley, K.A. (2006) The influence of natural radiation damage on helium diffusion kinetics in apatite. *Earth and Planetary Science Letters* 249, 148–161. https://doi.org/10.1016/j.epsl.2006.07.028

Sousa, F.J., Cox, S.E., Rasbury, E.T., Hemming, S.R., Lanzirotti, A., Newville, M. (2024) U and Th zonation in apatite observed by synchrotron X-ray fluorescence tomography and implications for the (U–Th)/He system. *Geochronology* 6, 553–570. https://doi.org/10.5194/gchron-6-553-2024

Willett, C.D., Fox, M., Shuster, D.L. (2017) A helium-based model for the effects of radiation damage annealing on helium diffusion kinetics in apatite. *Earth and Planetary Science Letters* 447, 195–204. https://doi.org/10.1016/j.epsl.2017.07.047